

Dual role of maleated polypropylene in processing and material characterisation of polypropylene /clay nanocomposites

Yu Dong ^{a,*} and Debes Bhattacharyya ^b

^a *Department of Mechanical Engineering, Curtin University of Technology
GPO Box U1987, Perth, WA 6845, Australia*

^b *Centre for Advanced Composite Materials, Department of Mechanical Engineering
The University of Auckland, Private Bag 92019
Auckland, New Zealand*

Abstract

Fundamental characterisation techniques were conducted with maleated polypropylene (MAPP) varying from 0 to 20 wt% (fixed clay content: 5 wt%) to understand its matrix plasticisation role in polypropylene (PP) /clay nanocomposites. It is evidently shown that well-balanced nanocomposite formulations with an optimal amount of MAPP no more than 6 wt% appear to be very critical.

Keywords: Nanocomposites; Nanoclays; Coupling agents; Mechanical properties; Matrix plasticisation

1. Introduction

Due to its enormous applications in automotive and packaging industries, PP is often embedded with a mix of clay agglomerates and partially intercalated/exfoliated clay platelets, which causes a moderate enhancement of mechanical properties compared to fully exfoliated nylon/clay nanocomposites [1-4]. Low interactions between hydrophobic PP molecular chains and hydrophilic clay platelets hinder the good clay dispersability level and thus could adversely affect the mechanical properties of nanocomposites. To overcome this difficulty, functional oligomers with polar groups like maleic anhydride grafted PP are generally added to cause the

* Corresponding author. Tel.: +61 8 92669055; fax: +61 8 92662681.
E-mail address: Y.Dong@curtin.edu.au (Y. Dong).

affinity for clay materials so that MAPP can serve as a “compatibiliser” between nanofillers and polymer matrix [2, 3, 5-7].

Early research work by Hasegawa et al. [5] shows that the tensile moduli of PP/clay nanocomposites are monotonically enhanced by increasing MAPP content up to 20 wt%. Whereas, controversial studies by Lee et al. [8], Chow et al. [9] and Dong et al. [6] indicate that increasing the amount of MAPP might not always lead to the continuous property enhancement of nanocomposites and there is a certain threshold above which the persistent increasing trend could be reversed. Furthermore, it has also been reported by Gicía-López et al. [10] and Dong and Bhattacharyya [1, 6] that impact strengths of PP/clay nanocomposites are continuously decreased in excess of MAPP. Thus, it is worthwhile to identify the significance of improving and achieving a good balance in the material properties.

The objective of this study is to investigate such a dual role of MAPP on the resulting mechanical properties of PP/clay nanocomposites in contrast to the clay dispersion so that the threshold level of compatibiliser can be systematically determined as the material formulation guidance to the nanocomposite manufacturers.

2. Experimental procedures

PP homopolymer SK H380F (melt flow index MFI=25 g/10 min) was supplied by Clariant (New Zealand) Ltd. NANOLIN™ DK4 organoclay (95–98% purified smectite content and interlayer spacing: $d_{001}=3.56$ nm), modified with octadecylammonium salt, was obtained from Zhejiang Fenghong Clay Chemicals, Co. Ltd, China. MAPP Exxelor™ PO1020 (MA content: 0.5–1 wt%, MFI=~430 g/10 min) was selected as the compatibiliser from ExxonMobil Chemical (Germany).

PP/clay nanocomposites were prepared by twin screw extrusion of PP and MAPP pellets with downstream clay feeding and then recompounded to extend the residence

time. Finally dried nanocomposites were injection moulded to prepare testing samples. The material preparation procedure and specifications were described in details elsewhere [6]. The nanocomposite formulations were based on varied MAPP contents from 0, 3, 6, 10 to 20 wt% (fixed clay content: 5 wt%).

Bruker D8 ADVANCE diffractometer was operated at 40 kV and 40 mA with Cu- k_{α} X-ray beam (wave length $\lambda=0.154$ nm). Both small and wide angle X-ray diffraction analyses were conducted to evaluate the intercalation effect of dispersed clay platelets ($2\theta=2-10^{\circ}$) and the crystalline structures of PP/clay nanocomposites ($2\theta=2-30^{\circ}$) at the scan rate of $0.4^{\circ}/\text{min}$, respectively.

Philips XL30S Field Emission Gun scanning electron microscope (SEM) was used at 5.0 kV to study the fracture morphology of nanocomposites. Cross section of injection moulded tensile sample in the longitudinal direction was obtained by cryogenic fracture in liquid nitrogen prior to the platinum sputter coating.

To examine the intercalated/exfoliated clay structures, Philips CM12 transmission electron microscope (TEM) was employed on the ultrathin nanocomposite samples (nominal thickness: 70 nm) with an accelerating voltage of 120 kV. Such TEM samples were cryogenically microtomed in the melt flow direction at -80°C with a Hitachi S-4700 ultramicrotome and collected on 300 mesh copper grids.

Mechanical properties were determined by using tensile, flexural and impact tests according to ASTM D638, D790 and D6110, respectively. A universal tensile machine Instron® 1185 was set up for tensile tests and flexural tests along with a laboratory-scaled three-point bending rig at room temperature. The Charpy impact strength was obtained by breaking notched injection moulded impact samples using a CEAST® Resil 25 pendulum impact tester.

Differential scanning calorimeter (DSC-Q1000 TA instrument, USA) was used for the assessment of thermal properties. The scanning temperature ranged from -60 to 220°C at the heating/cooling rate of $10^{\circ}\text{C}/\text{min}$. When heated up to 220°C , testing sample was kept in the isothermal condition for 5 min to eliminate any thermal history. The similar thermal cycle was run twice in a heating-cooling mode. The final melting and crystallisation curves were chosen from the first cooling and second heating scans, respectively. The melting temperature (T_m), crystallisation temperature (T_c) and degree of crystallinity (X_c) of the PP matrix in PP/clay nanocomposites were determined from the DSC measurement. X_c was calculated from the following relationship:

$$X_c (\%) = \frac{\Delta H_m}{(1 - W_f) \Delta H_f^0} \times 100 \quad (1)$$

where ΔH_m (J/g) is the heat of fusion of PP matrix, W_f is the weight fraction of clay particles and ΔH_f^0 is the heat of fusion of pure crystalline PP. ΔH_f^0 was assumed to be 209 J/g [11].

3. Results and discussion

3.1. Small angle X-ray diffraction (XRD)

Fig. 1 shows the effect of MAPP content on the clay intercalation level by XRD analysis. The first XRD peak intensities of all nanocomposites have greatly decreased, which indicates the reduction of existing clay tactoids. The peaks for PP/clay nanocomposites with low MAPP contents of 0 and 3 wt% appear to be shifted to slightly higher diffraction angles, implying the clay collapse structure possibly due to its low thermal stability [12] and surfactant degradation [13]. The presence of MAPP beyond 6 wt% gradually alleviates such adverse phenomenon with the peak-shifting to low angles for more evident intercalation at 10 wt% MAPP. However, the extent of

peak-shifting either to lower or higher diffraction angles is somehow insignificant, which could stem from the “skin-core” effect as previously mentioned in the other literatures [14-16]. The other plausible interpretation might result from the claim of effective intercalation mechanism [6]. Similar trend is also found for the second and third XRD peaks of PP/clay nanocomposites.

3.2. Fracture morphology and clay dispersion

Seen from SEM micrographs in Fig. 2(a), without the compatibiliser MAPP, the PP matrix is most likely to be surrounded by uncompatibilised large clay aggregates in size of around 2–3 μm apart from reasonable submicron sized clay dispersion. Clearly, the interfacial areas either present the partially embedding effect with small gaps between clay and PP matrix or completely become cavity-like voids due to the pull-out of clay particles, which means very weak interfacial interactions occurring in the absence of MAPP as the compatibiliser. With increasing the MAPP content, the clay particle sizes are significantly reduced and clay aggregates are separated into much thinner clay platelets ($<1\mu\text{m}$ in the lateral dimension) with a substantially improved interfacial adhesion. Furthermore, it is also observed that the higher the MAPP content is, the finer clay dispersion and smaller clay particle size are manifested, Fig. 2(b) – (e).

Direct observation for the clay dispersion state necessitates TEM analysis of PP/clay nanocomposites as shown in Fig. 3. When MAPP is not present, typical clay aggregates at a microscale level ($>2\ \mu\text{m}$) are widely revealed, Fig. 3(a). With existence of MAPP, the sizes of clay aggregates are significantly reduced and multiple intercalated clay platelets along with some individual exfoliated platelets are formed with a lateral dimension of 200–500 nm, Figs. 3(b) – (e). As expected, the degree of clay dispersion and the exfoliation level are enhanced with increasing the

MAPP content. Nonetheless, when the MAPP content is beyond 6 wt%, the morphological structures demonstrate that the clay dispersion level has not improved considerably, even though the higher MAPP content of 20 wt% offers slightly better dispersion, Figs. 3(c)-(e). This finding implies that an optimal MAPP amount of 6 wt% might be considered as the threshold level for balancing the compatibility and the resulting mechanical properties. Beyond this level, MAPP could play a matrix plasticisation role to soften overall nanocomposites as subsequently discussed, rather than acting as an effective compatibiliser.

3.3. Mechanical properties

Tensile and flexural moduli are initially increased with the addition of MAPP up to 3 wt%, but subsequently reduced while reaching 10 wt% MAPP, Figs. 4(a) and (b). After that they become more or less level-off with the MAPP content varying between 10 and 20 wt%, apart from slight variations that depend on the measured properties. With respect to tensile and flexural strengths, the maximum improvements have been found to be over 7 and 12% (MAPP content: 3–6 wt%), respectively, in comparison to those without MAPP. As a result, it is believed that the compatibility threshold level of MAPP content might be estimated in the range of 3–6 wt% where both tensile and flexural properties reach their highest levels. This finding coincides closely with the previous TEM analysis for the change of MAPP role from the compatibiliser to matrix plasticiser. Meanwhile, the tensile and flexural properties at a higher MAPP content (10–20 wt%) appear to be almost comparable to or slightly lower than those without MAPP due to such matrix plasticisation effect [6] though some property enhancements of PP/clay nanocomposites are still manifested compared to those of neat PP. As expected, the impact strengths are dramatically declined with increasing

the MAPP content, Fig. 4(c). At the lower MAPP content (0–3 wt%), a higher level of impact strengths is maintained with over 60% enhancement relative to that of neat PP. Initial impact strength improvement could be attributed to the size reduction of clay tactoids as well as a small amount of low molecular weight MAPP in the conventional polymer blending process. This indicates that clay dispersion has greater influence on the impact strength when the MAPP content is below the threshold level of 6 wt%. With increasing the MAPP content (≥ 6 wt%), impact strengths of nanocomposites diminish very drastically. In particular, when MAPP content reaches the highest level of 20 wt%, the impact strength of nanocomposites is even lower than that of neat PP. It is evidently proven that the matrix plasticisation role of MAPP becomes more predominant above the threshold as opposed to the uniform clay dispersion. The excessive amount of MAPP either stands alone due to multiple branching structures [17, 18] or is mixed with the PP matrix by mechanical shearing mechanism instead of being mobilised around the clay interlayer areas. Thus, the functionality of MAPP as the compatibiliser is inevitably worsened, reducing the material homogeneity with the enhanced brittleness nature [17, 18].

3.4. Wide angle X-ray diffraction (WAXD)

Fig. 5 shows the WAXD patterns for crystalline structures of PP/clay nanocomposites at various MAPP contents in comparison with those of neat PP and MAPP. Five characteristic peaks of the α -PP crystalline structure are observed in all the materials at 2θ angles of about 14.0, 16.8, 18.6, 21.2 and 21.9° corresponding to the lattice planes of (110), (040), (130), (111) and (131), respectively. For nanocomposites without MAPP, the other peak of β -PP structure is also identified on the lattice plane of (300) at 2θ angles of about 16.1°. β -PP structure can induce better impact resistance and greater elongation in comparison to α -PP [19, 20], in good

accordance with obtained higher impact strength of nanocomposites (MAPP: 0 wt%). In the presence of MAPP, β -PP structure completely disappears and the peak intensities of α (040) are significantly reduced when MAPP content is increased from 3 to 20 wt%. Since α -PP structure mainly contributes to the improvement of tensile modulus and better yield stress [19, 20], it is believed that at a fixed clay content of 5 wt%, increasing the amount of MAPP enables to prevent the further growth of α -PP, thus leading to the lower tensile properties of nanocomposites at a higher MAPP content.

3.5. Thermal properties

The melting and crystallisation behaviour of PP/clay nanocomposites at varied MAPP contents were characterised in DSC thermal analysis, illustrated in Fig. 6 and Table 1. The presence of 5 wt% clay particles and the increasing amount of MAPP in the PP matrix appear not to substantially influence both T_m and X_c . In relation to the crystallisation behaviour, the lack of MAPP as the compatibiliser (i.e. 0 wt% MAPP) has not hindered the nucleating role of clay particles but increased T_c considerably up to 121°C apart from much less favourable interfacial interactions. This phenomenon could stem from the well-known conventional heterogeneous nucleation effect for the generally used mineral fillers in polymer crystallisation. However, when increasing the MAPP content, a persistent decreasing trend of T_c is observed, which leads to the lowest T_c of 117°C for nanocomposites with 20 wt% MAPP ($T_c=113^\circ\text{C}$ for neat PP). The counteracting roles of clay and MAPP as positive and negative contributors to the nucleating effect might be worthwhile to propose to reflect the crystallisation behaviour of PP/clay nanocomposites. The excessive amount of MAPP with low crystallinity dispersed into PP matrix becomes quite detrimental to induce more nucleating cores and facilitate the crystallisation process since further improvements

of clay dispersion and interfacial interactions could be lessened beyond the MAPP threshold of compatibility.

4. Conclusions

The dual role of MAPP has made great impact on the clay dispersion, mechanical properties, crystalline structures and crystalline behaviour of PP/clay nanocomposites. Both intercalated and clay collapse structures are manifested in XRD analysis and the latter might be attributed to the clay thermal decomposition and surfactant degradation. The SEM analysis indicates that the presence of MAPP could enhance the uniform clay dispersion and achieve better interfacial adhesion between clay platelets and the PP matrix. Furthermore, a mix of partially intercalated/exfoliated clay formation is also identified by TEM observation with the threshold level of MAPP about 6 wt%, above which MAPP tends to be more like a matrix plasticiser to diminish the further improvement of mechanical properties of nanocomposites. For the crystalline structures of PP/clay nanocomposites, the peak intensities of α (040) in the α -PP formation have been reduced quite significantly due to the excessive amount of MAPP to hinder the growth of α -PP that can improve tensile properties of nanocomposites. The melting temperature (T_m) and degree of crystallinity (X_c) in the thermal properties of nanocomposites are marginally affected by the MAPP content. Nonetheless, despite the nucleation effect of clay with enhanced crystallisation temperature (T_c), increasing MAPP content results in such a persistent decreasing trend of T_c , which signifies the possible negative contributor of MAPP to the nucleation effect in the crystallisation of PP/clay nanocomposites.

Acknowledgements

The authors are grateful to New Zealand Tertiary Education Commission (TEC) and Foundation for Research, Science and Technology (FRST) under the grant No# UOAX0406 for financial supports.

References

1. Y. Dong, D. Bhattacharyya, P.J. Hunter, *Compos. Sci. Technol.* 68 (2008) 2864-2875.
2. Y. Wang, F.B. Chen, Y.C. Li, K.C. Wu, *Compos. Part B: Eng.* 35 (2004) 111-124.
3. F. Perrin-Sarazin, M.T. Ton-That, M.N. Bureau, J. Denault, *Polymer* 46 (2005) 11624-11634.
4. M. Alexandre, P. Dubois, *Mater. Sci. Eng.* 28 (2000) 1-63.
5. N. Hasegawa, M. Kawasumi, M. Kato, A. Usuki, A. Okada, *J. Appl. Polym. Sci.* 67 (1998) 87-92.
6. Y. Dong, D. Bhattacharyya, *Compos. Part A: Appl. Sci. Manuf.* 39 (2008) 1177-1191.
7. W. Lertwimolnun, B. Verges, *Polymer* 46 (2005) 3462-3471.
8. E.C. Lee, D.F. Mielewski, R.J. Baird, *Polym. Eng. Sci.* 44 (2004) 1773-1782.
9. W.S. Chow, Z.A. Mohd Ishak, J. Karger-Kocsis, A.A. Apostolov, U.S. Ishiaku, *Polymer* 44 (2003) 7427-7440.
10. D. Gicía-López, O. Picazo, J.C. Merino, J.M. Pastor, *Eur. Polym. J.* 39 (2003) 945-950.
11. J.E. Mark, *Physical Properties of Polymer Handbook*, AIP Press, New York, 1996.
12. J.W. Wee, Y.T. Lim, O.O. Park, *Polym. Bull.* 45(2000):191-198.
13. R.K. Shah, D.R. Paul, *Polymer* 47 (2006) 4075-4084.
14. D.H. Kim, P.D. Fasulo, W.R. Rodgers, D.R. Paul, *Polymer* 48 (2007) 5308-5323.
15. H.S. Lee, P.D. Fasulo, W.R. Rodgers, D.R. Paul, *Polymer* 46 (2005) 11673-11689.
16. D.H. Kim, P.D. Fasulo, W.R. Rodgers, D.R. Paul, *Polymer* 48 (2007) 5960-5978.
17. S.N. Sathe, G.S.S. Rao, K.V. Rao, S. Devi, *Polym. Eng. Sci.* 36 (1996) 2443-2450.
18. S.N. Sathe, S. Devi, G.S.S. Rao, K.V. Rao, *J. Appl. Polym. Sci.* 61(1996) 97-107.

19. S.C. Tjong, J.S. Shen, R.K.Y. Li, Polym. Eng. Sci. 36 (1996) 100-105.
20. J. Karger-Kocsis, J. Varga, J. Appl. Polym. Sci. 62 (1996) 291-300.

List of figures

Fig. 1 XRD patterns of DK4 organoclay and corresponding 5 wt% filled PP/clay nanocomposites.

Fig. 2 SEM micrographs of 5 wt% filled PP/clay nanocomposites at $\times 10000$ magnification with varied MAPP contents: (a) 0 wt%, (b) 3 wt%, (c) 6 wt%, (d) 10 wt% and (e) 20 wt%.

Fig. 3 TEM micrographs of 5 wt% filled PP/clay nanocomposites at $\times 15000$ magnification with varied MAPP contents: (a) 0 wt%, (b) 3 wt%, (c) 6 wt%, (d) 10 wt% and (e) 20 wt%.

Fig. 4 Mechanical properties of 5 wt% filled PP/clay nanocomposites: (a) tensile properties, (b) flexural properties and (c) Charpy impact strength.

Fig. 5 WAXD patterns of neat PP, MAPP and 5 wt% filled PP/clay nanocomposites. The curves are shifted vertically for clarity.

Fig. 6 Typical DSC curves of 5 wt% filled PP/clay nanocomposites: (a) heating scan and (b) cooling scan. The curves are shifted vertically for clarity.

List of Tables

Table 1 DSC characteristic parameters and level of crystallinity of PP/clay nanocomposites.

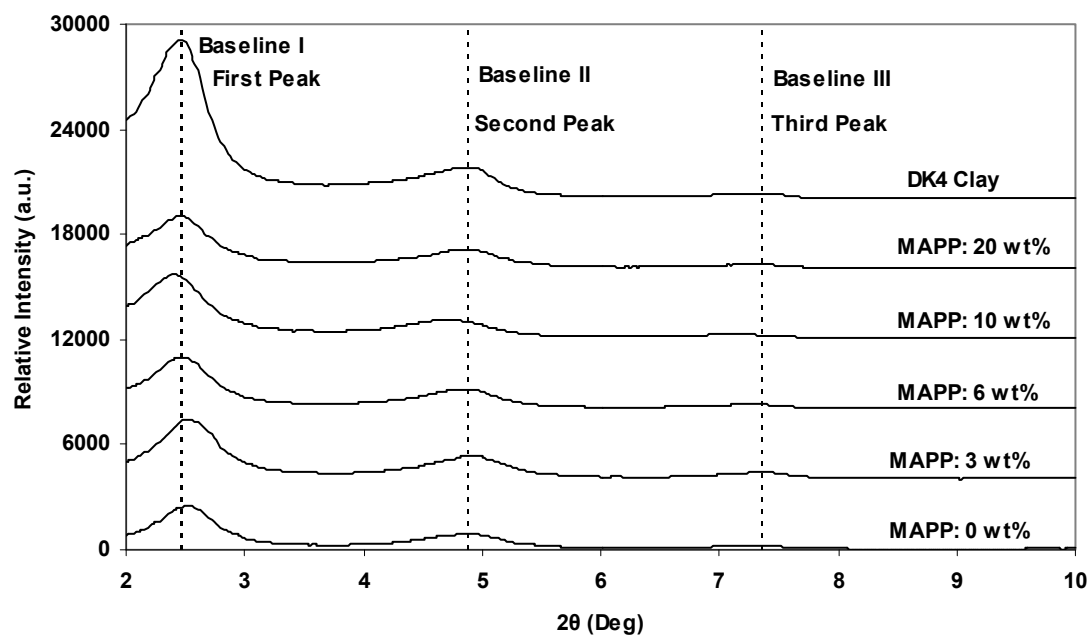
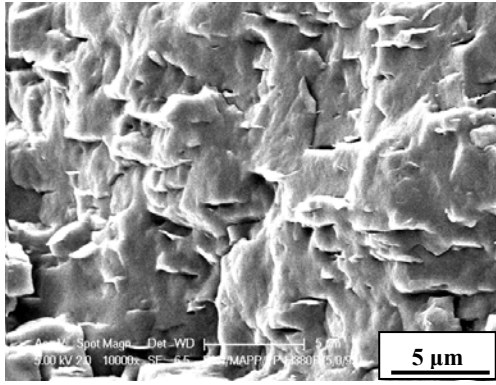
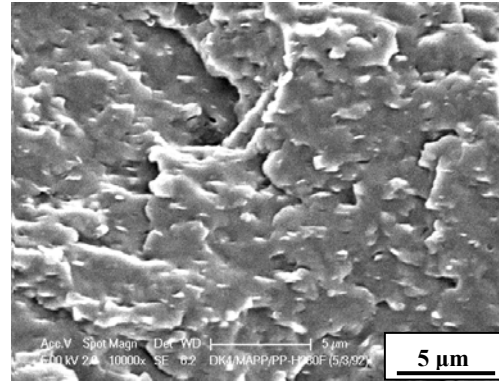


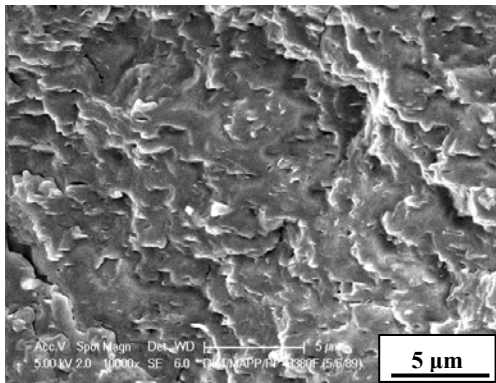
Fig. 1 XRD patterns of DK4 organoclay and corresponding 5 wt% filled PP/clay nanocomposites.



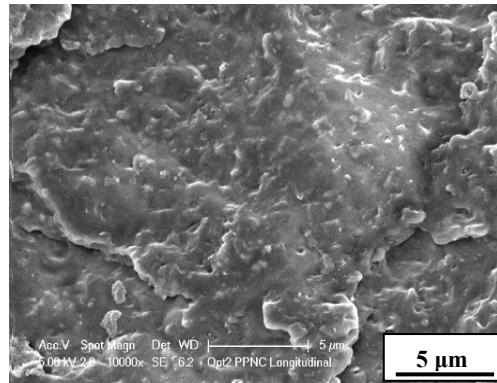
(a)



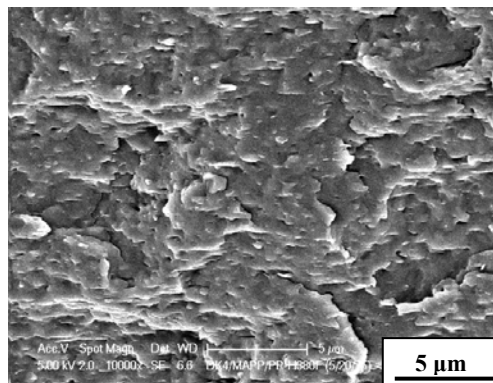
(b)



(c)



(d)



(e)

Fig. 2 SEM micrographs of 5 wt% filled PP/clay nanocomposites at $\times 10000$ magnification with varied MAPP contents: (a) 0 wt%, (b) 3 wt%, (c) 6 wt%, (d) 10 wt% and (e) 20 wt%.

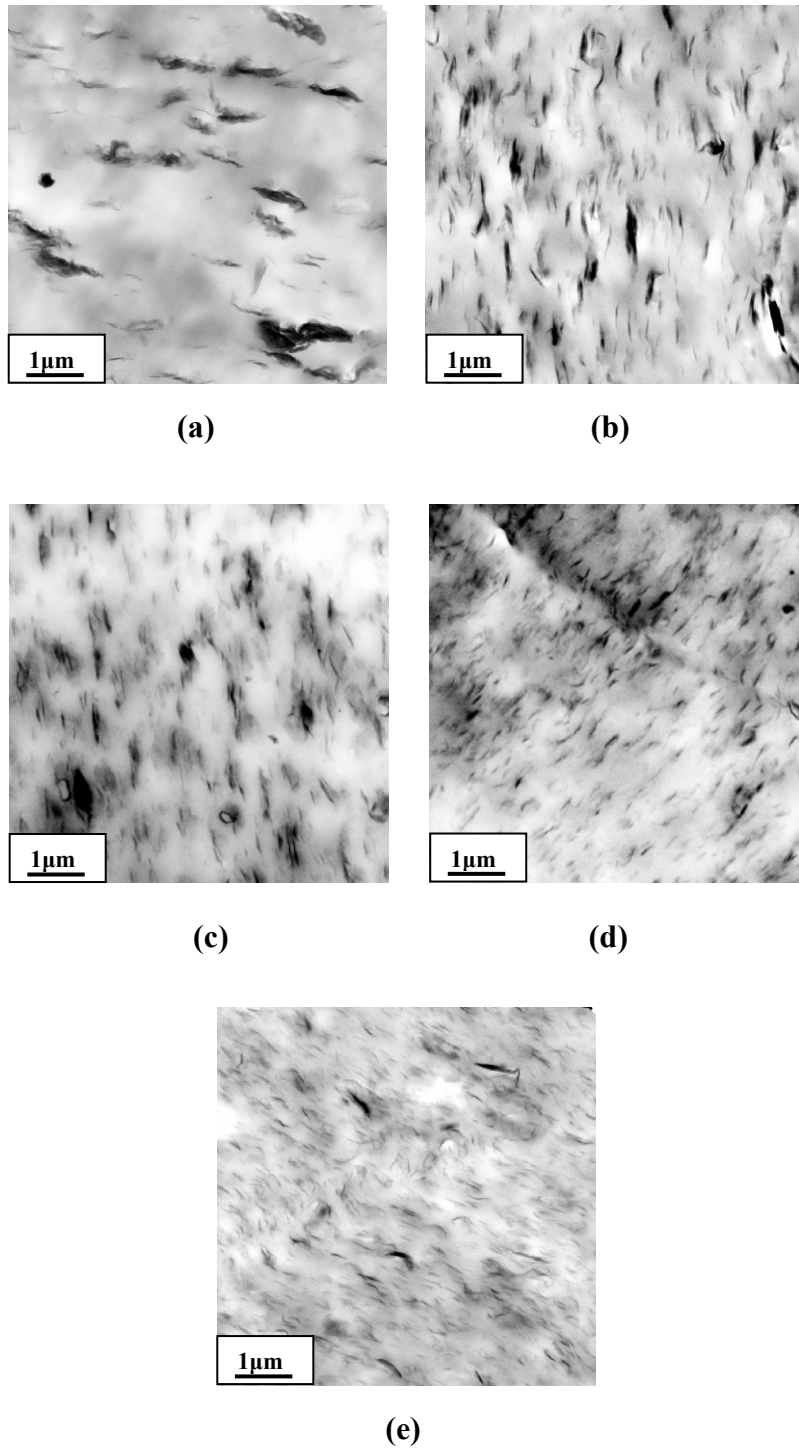


Fig. 3 TEM micrographs of 5 wt% filled PP/clay nanocomposites at $\times 15000$ magnification with varied MAPP contents: (a) 0 wt%, (b) 3 wt%, (c) 6 wt%, (d) 10 wt% and (e) 20 wt%.

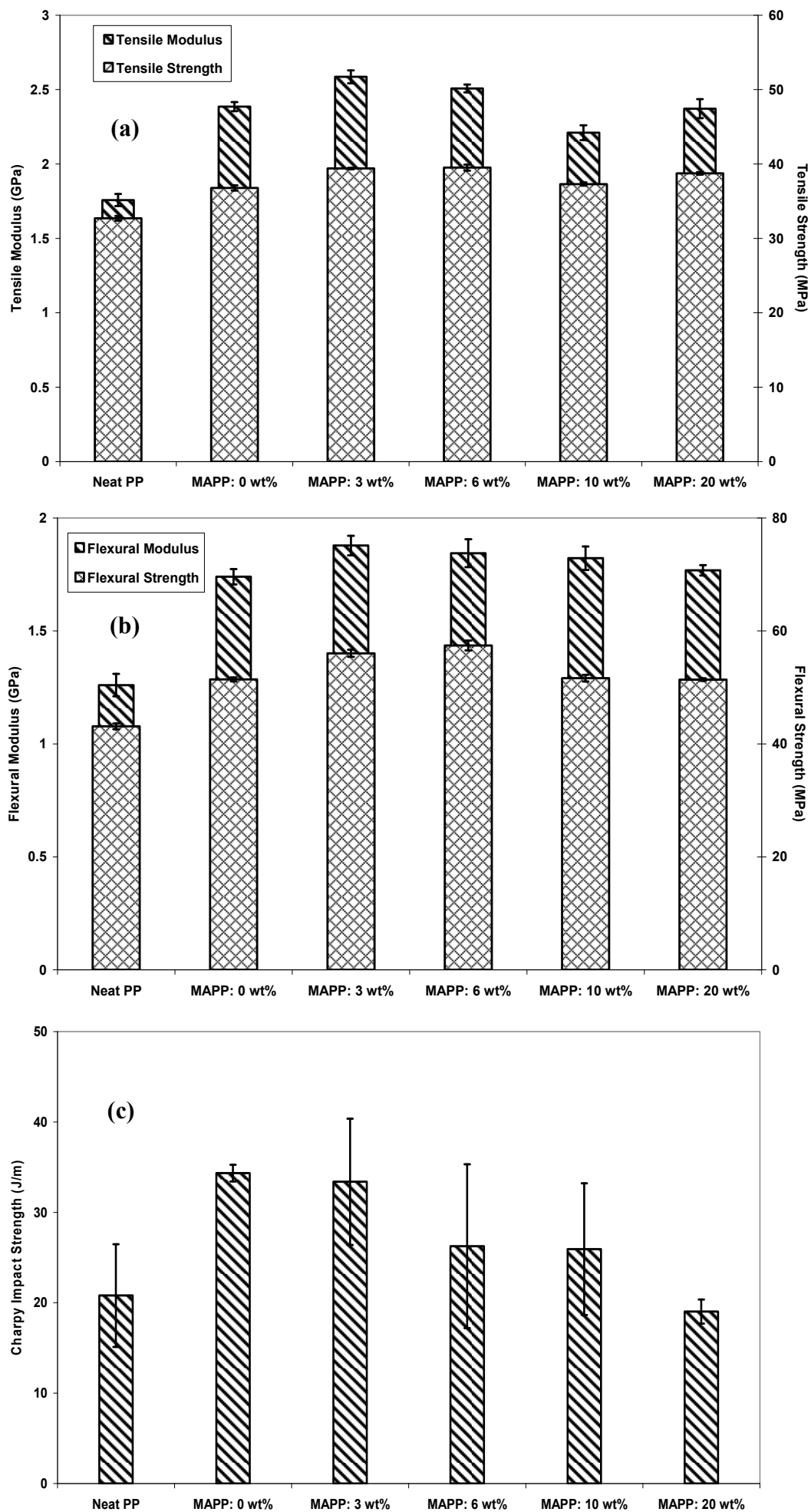


Fig. 4 Mechanical properties of 5 wt% filled PP/clay nanocomposites: (a) tensile properties, (b) flexural properties and (c) Charpy impact strength.

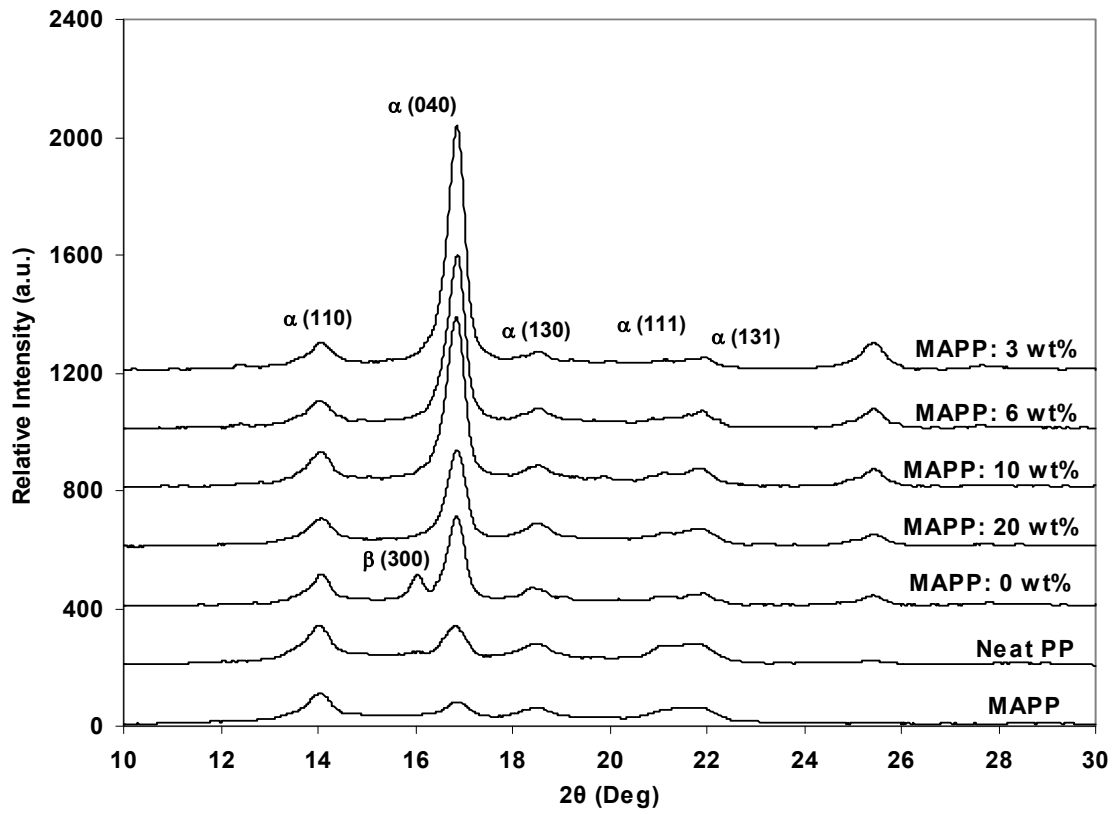


Fig. 5 WAXD patterns of neat PP, MAPP and 5 wt% filled PP/clay nanocomposites. The curves are shifted vertically for clarity.

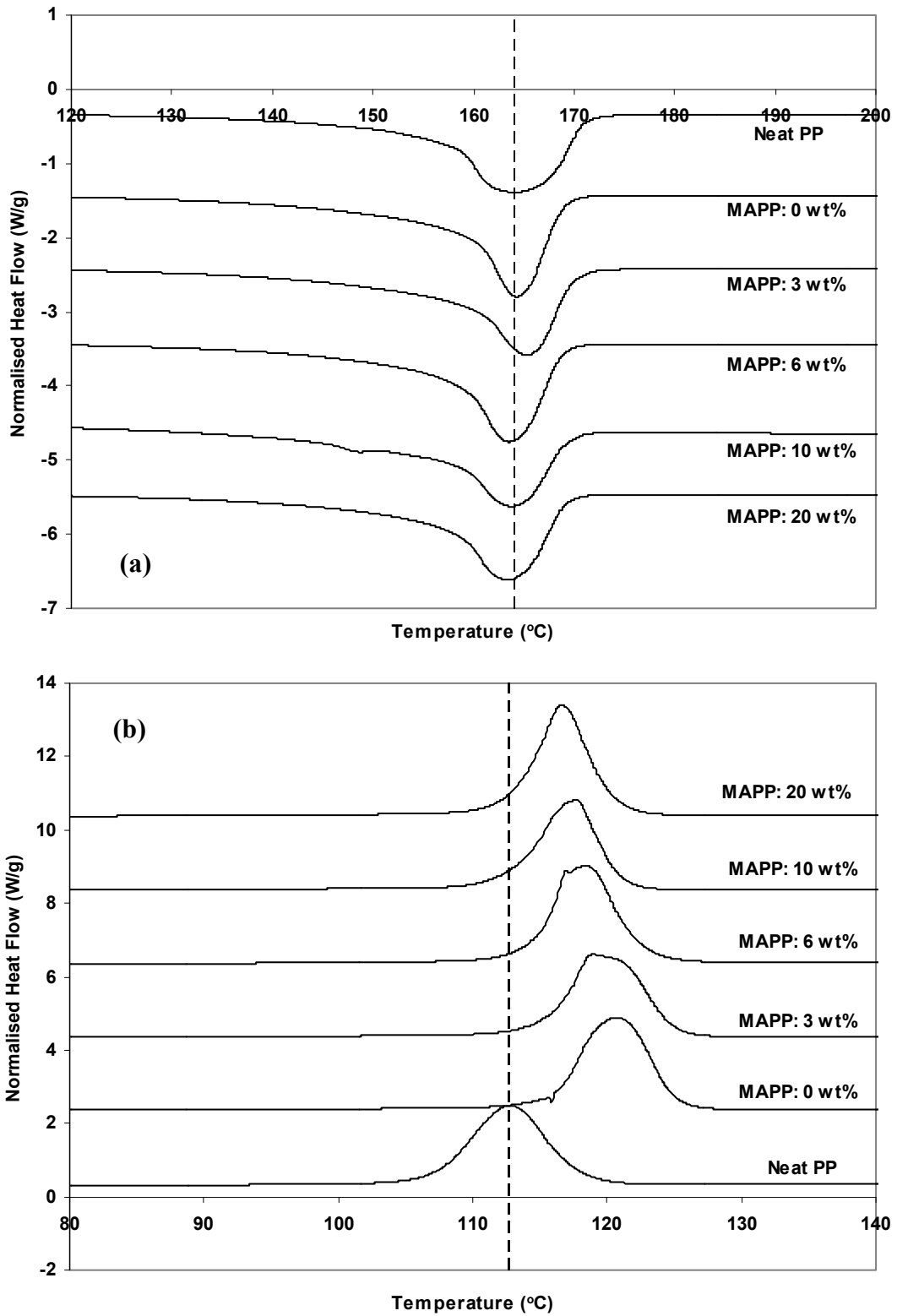


Fig. 6 Typical DSC curves of 5 wt% filled PP/clay nanocomposites: (a) heating scan and (b) cooling scan. The curves are shifted vertically for clarity.

Table 1 DSC characteristic parameters and level of crystallinity of PP/clay nanocomposites.

Material type	Clay /MAPP content (wt% /wt%)	T_m (°C)	T_c (°C)	ΔH_m (J/g)	X_c (%)
Neat PP	0/0	164.2	112.8	87.32	41.8
	5/0	164.3	120.7	90.08	45.4
Nanocomposites	5/3	165.3	119.0	86.20	43.4
	5/6	163.6	118.5	96.32	48.5
	5/10	163.9	117.7	89.06	44.9
	5/20	163.5	116.7	91.78	46.2